

Manuscript

Temporal and spatial variations of dust deposition along a Red Sea coastal section

Illia Shevchenko¹, Johann P. Engelbrecht^{1,2}, Suleiman Mostamandi¹, and Georgiy Stenchikov¹

¹King Abdullah University of Science and Technology (KAUST), Physical Science and Engineering Division (PSE), Thuwal, 23955-6900, Saudi Arabia.

²Desert Research Institute (DRI), Reno, Nevada 89512-1095, U.S.A.

Abstract

Wind-blown mineral dust as significant contributor of the atmospheric aerosols involved in multiple chemical and physical processes occurring in the atmosphere. Some of this processes and those impact in global energy budget, climatology, biogeochemical cycles, and health are known – other are the subject for the future research.

This work represents study of the mineral dust deposition samples collected around King Abdullah University Science and Technology (KAUST) campus from 2014 to 2019. 442 samples were collected and processed in 56 month sampling period. New sites for the frisbee type samplers were installed in different environmental domain, like islands in the Red sea and elevated roof top. Processing the samples is improved in comparison with previously described procedures (Engelbrecht et al., 2017). Sieving (56µm) was implemented for new samples starting May 2019 and for 38 previously processed samples. Gravimetric data and XRD mineral analyses result represented for listed samples. Particle size distribution analyses performed for listed samples with help of benchtop Malvern Mastersizer 3000® Laser Diffraction Particle Size Analyzer (LPSA).

Deposition data and size distribution of the samples compared with AERONET (AErosol RObotic NETwork) measurement from KAUST campus site.

Results of the Gravimetric measurements, XRD mineral analysis and size distribution applied for inter-comparison of sampling sites and efficiency of the used procedures in different local environmental obstacles and time period of the year.

Introduction

Mineral dust is ubiquitous in the earth's atmosphere, being emitted largely from continental arid and semi-arid regions of North Africa, the Middle East, and Asia, and to a lesser degree from Australia, southern Africa, south and north America (Prospero et al., 2002; Washington and Todd, 2005; Buseck et al., 2000; Goudie, 2006; Muhs et al., 2014; Edgell, 2006). The King Abdullah University of Science and Technology (KAUST) campus along the Red Sea coastal plain of Saudi Arabia is impacted by dust emissions and deposits from deserts of the Arabian Peninsula, and northeast Africa, with substantial dust contributions coming from the Red Sea coastal plain itself. The coastal plain is an important dust source region (Ginoux et al., 2012; Prospero et al., 2002; Anisimov et al., 2017; Prakash et al., 2016), the impact of which extends over the Red Sea. Dust sources impacting on the Arabian Red Sea coastal region were shown to vary by season, coming from local haboobs and low level jets delivering dust in part from the Tokar delta of Sudan in summer (Kalenderski and Stenchikov, 2016), and from the west coast of the Arabian Peninsula (Kalenderski et al., 2013).

Dust emission and dust deposition modeling supported by field sampling and measurements are required for the assessment of the dust mass budget. Both emission and deposition are not well constrained in atmospheric dust models, leading to large modelled uncertainties (Bergametti and Forêt, 2014; Schulz et al., 2012). To improve simulations, the establishment of continuous deposition networks in the vicinity of, and at distances away from dust sources, were suggested.

This study reported on here, follows on two recent related dust studies in the Red Sea coastal region, the first on the characterization of potential dust emission sources, and the second on the characterization of deposited airborne particulates over the Red Sea coastal plain. In the first study (Prakash et al., 2016), a set of 13 grab soil samples were collected at four localities from previously identified dust sources along, and adjacent to the Red Sea coastal plain. These samples were sieved and analyzed for particle size distribution, mineralogy, chemistry and particle morphology. In the second study (Engelbrecht et al., 2017), 52 monthly dust deposition samples were collected at four sites on the KAUST campus and adjoining locations, over a period of a year, in 2015. These samples were analyzed for deposition rate, and similar to the soil samples for their mineralogical content, chemical composition and particle size distributions.

This current study is an extension of the above mentioned two studies, providing gravimetric, mineralogical, and particle size information from six or more pairs of deposition samplers placed at strategically selected deposition sampling sites on the KAUST campus. The selection of the deposition sampling sites was decided upon to assess the compositional uniformity of the aerosol over KAUST from

which the deposition samples were being collected. Spatial differences in deposition magnitude and composition from local dust sources such as construction and road dust would also be identified. Multiple sampling sites also allowed for the identification of outliers from artifacts and other local anomalies.

Research topics being addressed here include an assessment of the deposition rates and dust compositions along and into the Red Sea, impacting on marine life and the ecology. This does not only depend on the amount of dust being deposited but also on the mineralogical and chemical composition as well as particulate sizes. Knowledge of the mineralogy of the sampled dust deposits will provide information on refractive indices, which can be used to calculate dust optical properties (Biagio et al., 2019; Kandler and Scheuven, 2019), providing input into radiative transfer models, and to better assess the impact of dust events along the Red Sea coastal plain. Further important implication of dust emission/deposition processes is associated with the harnessing of the solar renewable energy in the desert areas. Dust deposits on solar panels are known to have a severe detrimental effect on the efficiency of photovoltaic systems (Goossens and Van Kerschaever, 1999; Hamou et al., 2014; Mejia et al., 2014; Rao et al., 2014; Sulaiman et al., 2014; Ilse et al., 2016; Engelbrecht et al., 2017), with the severity of its adverse effects depending on dust mineralogy and climatic conditions.

With this study we were able to conduct detailed gravimetric, mineralogical and particle size analysis of deposition samples collected from the air over about a period of nearly five years.

Dust Composition

Dusts are composed largely of mixtures of fine airborne mineral particles, commonly including both individual and composite mineral grains. Minerals known to occur in continental soils from Middle East dust generating regions include quartz, feldspars, calcite, dolomite, micas, chlorite, kaolinite, illite, smectite, palygorskite, mixed-layer clays, vermiculite, iron oxides, gypsum, and halite (Engelbrecht et al., 2009a; Engelbrecht et al., 2016; Goudie, 2006; Prakash et al., 2016; Pye, 1987; Scheuven and Kandler, 2014). Depending on the composition of provenance rocks and local geology, the dust may also contain minerals such as amphiboles and pyroxenes. We show that similar mineral assemblages occur in variable proportions in the dust deposition samples collected on the KAUST campus and offshore.

The importance of dust mineralogy was long been recognized (Engelbrecht et al., 2016), but only recently the explicit transport of different mineralogical species is implemented in climate models (Perlwitz et al.,

2015a, b; Scanza et al., 2015). The mineralogy physical properties of dust generated from the Red Sea coastal region remains largely undocumented. The Red Sea coastal plain is a narrow highly heterogeneous piedmont area, and existing soil databases do not have the spatial resolution to represent it adequately (Nickovic et al., 2012).

Also, in the proximity of dust source regions such as the Red Sea arid coastal plain, deposition is a dominant process. The specific objective of the study reported on here is to examine temporal and spatial variability in mineralogical and morphological information of deposition samples collected on the KAUST campus. These results may help quantify the optical effects of dust blown across this region for nearly a five year period. We are presenting results from a network of deposition samplers located on the KAUST campus along the Red Sea coast of Saudi Arabia, and on two proximal offshore islands.

Methods

Deposition sampling

Sets of deposition samples were collected from six sites (Table 1, Supplement S1), on or close to the KAUST campus, each representing a different environmental domain. The goal for the distribution of the sampling sites was to assess the uniformity of the aerosol depositing dust by measurements at different sites, at ground level, elevated, and on two offshore islands. Pairs of samples were retrieved from the Frisby deposition gauges once a month. The first (NEO) was at an experimental solar panel site on campus, on a rock pebble covered yard with paved walkways. This site is being impacted by intermittent on-campus construction activities, and adjacent paved road vehicular traffic. The second site (CMOR) is set on a concrete quayside, approximately 5 meters from the seawall, subsequently impacted locally by the sea spray and activities along the quayside. The third site (Beacon) is on a small peninsular, partially surrounded by the sea, mangroves and dirt road, approximately 100 meters from the landmark KAUST beacon. The Al Misk site is on a small coral island, about 2 km off the KAUST campus coastline. The reasoning behind selecting this site was to have one site distanced from construction, roads or other local dust sources. This site, unfortunately, often produced samples contaminated by droppings from nesting Osprey, gulls, and seasonal flocks of migratory birds. This also resulted in algae growing in the plastic collection flask, more abundant in the higher rainfall months. A sampling site (Bld3roof) was set on the roof of a campus building, about 25 m from ground level, to provide samples at an elevation, vertically removed from local ground level dust sources and sea spray. A recent sampling site (Post) was set up on a second island about 1.5 km from the KAUST harbor, which, due to the harbor patrol

presence was expected to have less contamination from avian activities. The number of samplers at each site was standardized to two (Supplement S1).

At each sampling site, particulate deposits were collected by inverted Frisbee dust deposition gauges with open cell polyester foam inserts (Fig. 1) (Hall et al., 1993; Vallack and Chadwick, 1992, 1993; Vallack and Shillito, 1998; Engelbrecht et al., 2017; Vallack, 1995a; Vallack, 1995b). The deposition samples were accumulated over a period of one calendar month. They were retrieved from the deposition gauges by thoroughly flushing the particulates from the foam insert into the Teflon coated aluminum dish with distilled water dispensed from a pressurized spray bottle. In this fashion the slurry and dissolved deposition sample is quantitatively deposited into the inverted Frisbee dish, down the plastic tube and into the white plastic sample collecting bottle. Once a month, and with each sample collection, a new polyester foam insertion as well as a thoroughly rinsed out collecting bottle, is installed. These precautions are to minimize any cross contamination of sequential samples. In time the foam inserts became decomposed and brittle from the UV sunlight, and if not replaced regularly (monthly), resultant small flakes of the polyester foam landed in, and contaminated the sample.

A total of 442 deposition samples (Table 1) were collected and weighed over the campaign period of 56 months, from December 2014 to December 2019. Since we previously (Engelbrecht et al., 2017) reported on samples collected in 2015, this paper presents results largely for the period May 2016 to December 2019, when the particle size distributions was measured.

Sample retrieval and analysis

To eliminate non-aerosol artifacts such as coarse sand pebbles, plant material, bird detritus, plastic foam chips, and algal blooms, the deposition sample slurries are passed through a 56 μ m stainless steel screen. The sieved sample was thereafter transferred to half fill a 600 or 900 ml freezer flask. The flask with sample is chilled in two steps, first to about < 40 °C by rolling in a chilled ethanol bath in a “shell freezer”, and thereafter to about <70 °C in an upright freezer. This two-stage freezing process takes about two days and was found to best avoid shattering of the glass freezing flask, and subsequently also the loss of the deposition sample. The glass flask with frozen sample is connected to a vacuum system to sublimate the sample to dryness over a period of another about two days. The freeze-dried (sublimated) sample is transferred to a test tube for subsequent mass measurements, mineral analysis by powder X-

ray diffraction (XRD), and LASER particle size distribution analysis (LPSA). The samples collected for the period May 2019 to December 2019 were sieved to $<56\ \mu\text{m}$ directly after being collected in the field. A subset of about 38 samples collected in the period May 2016 to September 2018 had not been sieved immediately after being collected, and were later re-suspended in distilled water, sieved and weighed a second time as discussed in detail below. This was done to remove artifacts and coarse mineral grains found in some earlier samples. The sample loss from the re-suspension and sieving process is considered to be less than 10% for samples that do not contain large amounts of artifacts (Supplement S10).

Gravimetry

Subsequent to freeze-drying, the samples are weighed on a five decimal laboratory balance. Together with the known diameter of the Frisbee sampling gauge (227 mm) the deposition rates in grams per square meter per month ($\text{g m}^{-2} \text{mo}^{-1}$) were calculated. A summary plot of the monthly averaged total deposition rates as well as standard deviations of the monthly means are shown in Fig. 2, with the individual histogram plots shown in Supplement S2.

Mineral analysis by X-ray diffractometry (XRD)

Measurement of the mineralogical content of dust is necessary to assess its radiative effect. Optical properties including scattering and absorption depend on the real (n) and imaginary (k) parts of the complex ($m = n + k$) refractive indices of minerals and other phases contained in the dust mixture. For a given mineral particle size and particle shape, the refractive indices also vary by wavelength. X-ray diffractometry (XRD) is the commonly applied technique for the measurement of the mineralogical content of dusts. No composition references or standards were used in this procedure, and XRD results should be considered semi-quantitative at best. Depending on the mineral crystallinity and sample preparation procedure, minerals at concentrations less than about 3% cannot be accurately measured by XRD. We applied the relative intensity ratio (RIR) method after Chung (1974), whereby the measured mineral concentrations are normalized to 100%. This method also excludes concentrations of amorphous and low crystalline phases, including volcanic glass and organic compounds. The accuracy of the measurements is also detrimentally affected by diffraction peak on peak and peak on background interferences, preferred orientation in the sample mounts, and variable crystallinities of the minerals.

Approximately 0.25 g of the sample was lightly loaded into a front-loading sample holder, taking care not to press down onto the sample, so minimizing preferred orientation of the platy mineral particles. The powder sample mounts were run on a Bruker D8 powder diffractometer operating a Cu anode tube at 40 kV and 40 mA. Scans were collected over a range of 5° to 75° in steps of 0.01° 2 θ, for about 120 minutes per scan.

The XRD intensities were processed to provide the semi-quantitative mineral concentrations, applying the Bruker AXS X-ray DIFFRAC EVA software together with the International Centre for Diffraction Data, ICDD PDF-4/Minerals data base.

Positive Matrix Factorization (PMF)

Positive Matrix Factorization (PMF) is a multivariate factor analysis technique for evaluating large environmental data sets, providing a method for receptor modeling whereby aerosol source types can be fingerprinted and source attributions modelled (Paatero and Tapper, 1994; Norris et al., 2014; Comero et al., 2009).

The model can be expressed as:

$$X = GF + E$$

Where X is then measured data matrix, in this case the mineralogical compositions, G and F are the matrices to be determined and E is the residual matrix. G is the source attributions matrix and F the matrix characterizing each source type, i.e. the mineralogical source fingerprint of each source. The elements of both G and F are constrained to be positive, implying that emitting sources cannot have negative mineral concentrations. The iterative process strives to minimize errors in E.

Particle size analysis

Aerosol particle size distribution is considered to be one of the most important physical parameters, largely due to its radiative effect (Scheuven and Kandler, 2014; Highwood and Ryder, 2014; Miller et al., 2014), and has also been extensively studied for its health effects (Morman and Plumlee, 2014), and cloud formation processes (Nenes et al., 2014). To measure particle sizes of dusts is complicated by the fact that the particles often aggregate to form multi-mineral clusters. The occurrence of surface coatings of individual minerals such as clays, iron oxides, carbonates and evaporites on harder minerals such as

quartz and feldspars (Engelbrecht et al., 2016) is common. Also, the individual minerals can vary in shape, with variable aspect ratios, from near spherical for feldspar and quartz grains, to platy particles such as clays and micas (Scheuven and Kandler, 2014).

The particle size measurements were performed on a benchtop Malvern Mastersizer 3000[®] Laser Diffraction Particle Size Analyzer (LPSA) equipped with a Hydro LV liquid sampling unit, and Standard Operating Procedure (SOS) software package customized to the analysis of particle suspensions in the 0.1-1000 μm diameter range. The instrument measures blue and red wavelength scattered laser intensities, and applies software to calculate the volume percentages of the particle size bins, assuming the particles to be perfect spheres as per the Mie theory. The blue laser is particularly suited for particles below 1 μm in diameter and the red laser for larger diameter particles.

Approximately 150 mg of freeze-dried sample is added to 10 ml aqueous solution of 0.1 % sodium hexa metaphosphate de-flocculant in a test tube. The suspension is gently shaken overnight before pouring into a 600 ml glass beaker of distilled water. The beaker with suspension is placed on the liquid sampling unit and sonicated for 90 seconds to de-aggregate the mineral clusters which had formed with the sampling and freeze-drying steps, before starting the measurement cycle. The sample is kept agitated while being pumped into the system for measurement in five consecutive cycles.

Results

Gravimetric results

Gravimetric results covering the total deposition sampling period, December 2014 – December 2019 are graphically represented as histogram plots in Supplement S2. Outliers are attributed to artifacts from resident Osprey and migratory bird swarms contaminating and damaging the deposition samples in the Frisby dishes. This occurred routinely at the Al Misk island site (March, April and May, December 2018; February 2019) and sometimes the Post island site (February, April 2019). These samples were either voided, or if recorded, not included in the calculation of the deposition rate means and standard deviations (Fig. 2, Supplement S2). Anomalously high deposition rates are also ascribed to sea spray

during stormy conditions such as at the CMOR quayside (October, September 2015), and Beacon (April, December 2016) site, and locally generated construction dust at the NEO sampling site (August 2015, April 2017). In general, anomalous measurements not included in the calculation of the average monthly deposition rates and standard deviations, are those that fall outside about twice the standard deviation of the mean for that month.

The monthly average deposition rates varied substantially, from as low as 3.6 g m^{-2} in June 2016 to as high as 25.2 g m^{-2} in November 2017. Although not consistently the case, the lowest deposition rates occurred mostly during the Summer months of June, July and August. In contrast, high deposition rates occurred frequently in the months of September until February. The annual deposition rates for the five sampling years varied, being $13.4 \text{ g m}^{-2} \text{ mo}^{-1}$ in 2015, $11.4 \text{ g m}^{-2} \text{ mo}^{-1}$ in 2016, $11.5 \text{ g m}^{-2} \text{ mo}^{-1}$ in 2017, $12.2 \text{ g m}^{-2} \text{ mo}^{-1}$ in 2018, and $7.6 \text{ g m}^{-2} \text{ mo}^{-1}$ in 2019.

Inter-comparison of sampling sites

The goal is to establish if all six sites should be retained to provide a representative deposition sample from the KAUST atmosphere. As described above, there are continuous unresolved issues with monthly samples from the two island sites, and periodically, to a much lesser extent from some of the four land-based sites. The two samplers close to the seashore, and one to two meters above sea level, are occasionally impacted by sea spray. The deposition sampling at the DT3 NEO (Solar) site was disrupted for a six-month period, July to December 2019 due to local on-campus construction activities. A comparison was made between the mass collected at the two shoreline (CMOR, Beacon) and the recent (since May 2019) elevated rooftop (Bld3roof) sites?

An analysis of variance (ANOVA) was performed on a subset of measurements from the three land-based sampling sites, for the period May 2019 to December 2019. Requirements for the ANOVA are that the data be normally distributed about the sample means, and for the three data sets to have similar variances. Histogram plots (Fig 3) showed the mass data to be positively skewed. An approximate normal distribution of the gravimetric data was produced by performing a logarithmic transformation on the original measured results (Fig. 3 a, b, Table 2).

The F-tests involved a first stage whereby the variances of the three land-based sample sets were compared followed by an analysis of variance on the three logarithmic transformed data sets (Table 3). The measured F values of the sample pairs are close to unity, varying between 1.028 and 1.065, well

below the tabulated F critical value of 2.46, implying that the three logarithmically transformed data sets have similar variances at a 5% level of significance, the null hypothesis $H_0: \sigma_1^2 = \sigma_2^2 = \sigma_3^2$ is not rejected. (Supplement S4).

An analysis of variance (ANOVA) (Table 4) was subsequently performed on the three logarithmically transformed three data sets (Table 4, Supplement S4). The calculated F value of 0.776 in this case is well below the F critical value of 3.209 at the 5% level of significance, showing that the null hypothesis $H_0: \mu_1 = \mu_2 = \mu_3$ could not be rejected, implying that the three population means are similar to each other.

In summary the F tests show that the aerosols measured at the three sampling sites are similar, regardless of locality or elevation. It can be suggested that there is no benefit to having three land-based sampling sites. The sampling site on the roof of the building (Bld3roof) maybe the best selection since it is not as much impacted by occasional sea spray, construction, or other Intermittent local dust producing activities. Similarities amongst the three sites were also found for the $\leq 20 \mu\text{m}$, $\leq 10 \mu\text{m}$ and $\leq 2.5 \mu\text{m}$, size fractions (Supplement S4).

Mineralogy by XRD

Semi-quantitative mineral analysis by XRD was performed on about 138 monthly deposition samples for the period May 2016 to December 2019 (Supplement S5) collected at the six sampling sites. These were generally sieved through a metal screen to $< 56 \mu\text{m}$, to separate out and discard any large mineral grains, artifacts and algal blooms that may have grown in the sampler collection flask.

The major silicate minerals in the samples are quartz ($22.18 \pm 6.17\%$) and feldspar ($18.71 \pm 5.22\%$) (Table 5), with lesser amounts of mica ($12.34 \pm 3.83\%$), clay (kaolinite ($6.12 \pm 2.02\%$), illite ($5.07 \pm 2.52\%$)) chlorite ($5.86 \pm 2.01\%$) and hematite ($1.19 \pm 0.7\%$). The carbonates (calcite ($2.52 \pm 1.44\%$), dolomite ($2.21 \pm 1.02\%$)) and gypsum ($8.44 \pm 3.25\%$) are present in small amounts, together with halite ($15.41 \pm 9.91\%$), most likely from intermittent storms transporting sea spray. Similar to the gravimetric data, most of the mineral concentrations including of the feldspar, clays, chlorite, hematite, carbonates and gypsum, have positively skewed distributions (Supplement S6). In contrast, quartz is negatively skew, alluding to a deposition rate, different to those of the other silicates such as the felspars and clay minerals with which it is normally associated. Halite shows a uniform distribution pattern, dissimilar to the lognormal distributions of the silicates. This is suggested to be that rainstorms carrying dissolved sea salt occur sporadically but at high concentrations, unassociated regular daily dust deposition.

The correlation coefficients for the mineral species (Table 6) supports some of the findings drawn from the above mineral distribution data. Due to the large uncertainty of concentration measurements by XRD, the correlation coefficients are small, most in the -0.5 to 0.4 range. Exceptions are the 0.59 for the gypsum-calcite and -0.6 for the halite-feldspar association.

Quartz and feldspar are positively correlated with each other but unexpectedly negatively correlated with the other dust components such as the clay mineral illite, the oxide hematite and the carbonates (dolomite and calcite). This may be interpreted to mean that there are two mutually exclusive dust types, the one of coarse grains of quartz and feldspar, and the other largely of clays, carbonates and oxides. It is suggested that the two dust types represent two different atmospheric conditions, one high wind transporting and depositing larger grains of quartz and feldspar, and the other moderate wind conditions with more fine clays and carbonates, and less quartz and feldspar. This is further confirmed by the positive correlations amongst the clay minerals kaolinite and illite and chlorite, and the carbonates calcite and dolomite.

Halite is negatively correlated with all the silicate and carbonate dust minerals. This can be explained by winds from the Red Sea containing largely sea salt but little or no crustal dust, while winds on land along the coastal plain bears no or little sea salt on average and largely crustal minerals.

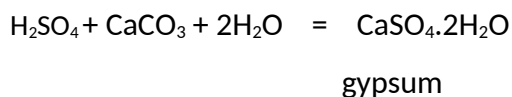
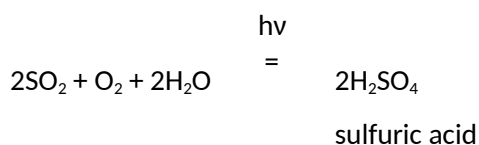
The larger correlation between gypsum and calcite on closer inspection turned out to be due to the (-2;4;1) diffraction peak of gypsum (at $29.20^\circ 2\theta$) overlapping with the (1;0;4) diffraction peak of calcite (at $29.12^\circ 2\theta$). Since neither interference nor other standards were measured in our analysis, we did not correct for this interference, resulting in an overestimation of the calcite mineral concentration and the positive correlation of 0.59.

To further understand the mineral interrelationships the data were subjected to PMF modelling. A modelled four factor solution provided factors which can be explained in terms of known particle source types, such as crustal dust and marine sea salt. Each factor could be assigned a source type name, depending on the mineral content of the factor (Table 7) (Engelbrecht and Jayanty, 2013). By far most of the halite (70.82%) occurs in Factor 1 and is assumed to be largely of marine origin. The clay components such as kaolinite (52.91%), illite (61.05%), and chlorite (50.60%) as well as the hematite (64.47%) are contained in Factor 2 (clay). This Factor 2 also contains an unexplainable high percentage of feldspar. Factor 3 contains the largest amounts of gypsum (74.36%) and the carbonates calcite (63.68%) and dolomite (32.65%), and is labelled gypsum-carbonate. Most of the quartz (61.93%) is contained in Factor 4, together with some clay minerals and is labelled quartz. All four modelled PMF

factors also contain lesser amounts of the other minerals. These mineral profiles can be considered to represent fingerprints of dust types impacting on the sampling sites (Engelbrecht and Jayanty, 2013). Source attributions, whereby the contribution of each factor to a sample was calculated (Supplement S7). Here source profiles and the source attributions are ill-resolved for several reasons, the most important being that the deposition samples were collected over a period of a month, during which time the emission rates of dust and other pollutant sources, and meteorological conditions varied. Further sources of error are related to the deposition sampling in the field. Inaccuracies of XRD diffraction peak measurements are related to diffraction peak overlaps, preferred mineral orientation, crystallinity, and the fact that mineral concentrations less than about 5% are difficult to measure by XRD with any degree of certainty.

Regardless of the above experimental errors, some qualitative interpretation can be given to the four modelled factors. Factor 1 (marine) represents dust blowing from the sea, factor 2 fine clay rich dust occurring under prevailing wind conditions, factor 3 a gypsum and carbonate rich source, and factor 4 coarse particles of quartz being transported onto the KAUST campus during stronger wind conditions. No seasonal fluctuations could be seen from the source attributions (Supplement S7).

The positive gypsum-carbonate relationship shown in Tables 6 and 7 can at least in part be due to a close mineralogical association of the gypsum, calcite and dolomite, although there may be an overestimation of the calcite due to a measurement discrepancy, as explained above. It is suggested that the gypsum is a reaction product of carbonate such as calcite (CaCO_3) and dolomite ($\text{CaMg}(\text{CO}_3)_2$), with sulfur dioxide (SO_2) from industry, under favorable photochemical and humidity conditions.



A similar reaction is suggested for dolomite ($\text{CaMg}(\text{CO}_3)_2$)

The formation of gypsum is likely to have formed in the ambient atmosphere before deposition, although it can also occur after deposition of the carbonate dust in the Frisby samplers. An exploratory investigation did show recrystallization of gypsum on exposed surfaces (Engelbrecht et al., 2017).

Particle size distributions

Particle size analysis was retro-actively executed on a subset of 38 samples covering the period May 2016 to September 2018. The samples were analyzed twice for particle size, once on samples as collected in the field, and a second time after wet sieving the samples to $<56 \mu\text{m}$ (Supplement S8). Thereafter all samples, including 78 samples collected in the period May 2019 to December 2019 were sieved to $<56 \mu\text{m}$ prior to the freeze drying and particle size measurement (Supplement S9), i.e. a total of 116 collected deposition samples were analyzed for their particle size distributions. From the cumulative volume densities and the total mass, deposition rates for any measured size fraction can be calculated, e.g. $\leq 20 \mu\text{m}$, $\leq 10 \mu\text{m}$, or $\leq 2.5 \mu\text{m}$ (Supplements S10, S11).

Unless contaminated by algae or locally generated large sand particles or detritus, the size distributions for the unsieved and sieved samples are similar in volume density and size class. The size distributions are always bimodal with a small volume percentage representing the fine mode, at less the $1 \mu\text{m}$ and a substantially larger volume percentage in the $1 \mu\text{m}$ to about $126 \mu\text{m}$ bin range, and a mode at about $25 \mu\text{m}$, representing the coarse mode. To avoid larger non aerosol artifacts, all samples for the months of May to December 2019 were sieved through a $56 \mu\text{m}$ stainless steel screen.

Based on the data from the two cycles of particle size measurements on the 38 samples, an assessment was made of sample loss from the additional second cycle of measurements. Average volume distribution and cumulative distribution plots for the unsieved and $<56 \mu\text{m}$ sieved sample sets are shown in Fig. 4 (a, b). The contribution of particles larger than $100 \mu\text{m}$ is greatly reduced by the $56 \mu\text{m}$ sieve. Superimposing the average volume distribution plots (Fig. 5) of the sieved and unsieved sample sets shows, as expected the exclusion of the larger particle fractions and the shift of the distribution curve towards the smaller particle fractions. The magnitude of displacement varies by particle size. The volumetric percentages of the three particle sizes $\leq 20 \mu\text{m}$, $\leq 10 \mu\text{m}$, and $\leq 2.5 \mu\text{m}$ are as expected greater for the sieved samples than for the unsieved samples (Table 8). The $\leq 2.5 \mu\text{m}/\leq 10 \mu\text{m}$ ratios of 0.19 and 0.2 for the sieved and unsieved samples can be considered as proxies for $\text{PM}_{2.5}/\text{PM}_{10}$ ratios measured in ambient samples and on the low end of $\text{PM}_{2.5}/\text{PM}_{10}$ ratios normally measured on ambient samples from the Middle East (Engelbrecht et al., 2009). The lowest average value for $\text{PM}_{2.5}/\text{PM}_{10}$ of 0.21 was

measured at Tallil in Iraq. The majority of the other sites measured in the region had $PM_{2.5}/PM_{10}$ ratios in the 0.3 to 0.4 range. However, it can be expected for deposition samples to have less fine dust than ambient samples.

Comparative distribution plots show that in general approximately 30% by mass of the deposition samples was discarded by the sieving process (Fig 6 (a)). The mass losses from sieving were on average 20% for $\leq 20 \mu\text{m}$ (Fig 6(b), 10% for $\leq 10 \mu\text{m}$ (6(c)), and 11% for $\leq 2.5 \mu\text{m}$ (Fig. 6(d)). The differences can be attributed to severe dust events depositing large mineral particles and detritus from local sources close to the samplers during wind gusts, artifacts dropped onto the sampling dish by birds, algae growth in the sampling bottle following rainstorms, and sample collection and preparation losses.

Discussion and Conclusions

There were monthly fluctuations in deposited mass by the depositional samplers, more evident in 2015 (Engelbrecht et al., 2017). In that year the highest deposition rates were recorded in Spring and Fall and the lowest in Summer. On average, this deposition pattern occurred in the 2016 to 2019 years, with the lowest deposition rates in the periods June through August and the highest from September to February.

The six sites, four on land and two on islands, as well as the one site on land at elevation did not show any significant differences in deposition rates, pointing to the homogeneity of the aerosol over the sampling region. This weighs on the decision to henceforth confine deposition sampling to one land-based site.

Semi-quantitative XRD showed a consistency in mineralogical content of the dust samples, should the sea salt and local construction dust be disregarded. The major minerals in all samples are quartz and feldspar, with lesser amounts of various clays, hematite, carbonates and gypsum. Gypsum can in part be considered a reaction product of calcite and dolomite, with sulfur dioxide possibly from industrial sources. PMF modeled source profiles of the mineralogical abundances distinguished the gypsum-carbonate as a separate source type, alluding to periods during which gypsum may have formed in the ambient atmosphere. It should also be borne in mind that some of the gypsum may have come from gypsum bearing soils (Engelbrecht and Jayanty, 2013).

AERONET Measurements

Deposition measurements were compared to monthly averaged measurements collected at the AERONET measuring site on the KAUST campus.

Aerosol Optical Depth

There are substantial gaps in the AOD data with 42 out of the total of 62 months blank (Supplement S13) collected for the period December 2014 to December 2019. The correlations between the deposition rates and the AOD measurements are weak, as can be seen in a scatter plot (Fig. 9), with R^2 of 0.0092 and a linear correlation coefficient of 0.096. Supplement S13 shows the deposition rate and AOD on a single plot. In some areas it seems as if there is a correspondence but for other months the measurements are somewhat displaced.

Particle size distributions

Monthly averaged particle size distributions of aerosols from AERONET (Müller et al., 2012) were compared with particle size distributions of deposition samples measured optically by Laser diffraction (Malvern Mastersizer 3000) and by electron microscopy (Engelbrecht et al., 2017). Over a time interval of 44 months, spanning May 2016 to December 2019, 19 sets of monthly averaged particle size distributions were retrieved from AERONET (Supplement S11). All particle size distributions show distinct bi-modal volume distributions with the minor (fine) modes at about 0.26 μm particle diameter and the major (coarse) mode at about a particle diameter of 4.5 μm (Fig 7). The local minimum for all 19 sample sets is consistent at a particle diameter close to 0.88 μm , being the separation diameter between the fine and coarse modes.

The cumulative distribution (Fig.7) provides a convenient tool for the assessment of volume percentages of particle diameters between 0.1 and 30 μm . Table 9 provides the average volume percentages of $\leq 10 \mu\text{m}$ of 95.86%, $\leq 2.5 \mu\text{m}$ of 39.0%, $\leq 0.88 \mu\text{m}$ of 23.66%, as well as the volume fractions $\leq 10 \mu\text{m} : \leq 2.5 \mu\text{m} : \leq 0.88 \mu\text{m}$ of 1 : 0.42 : 0.25, together with the standard deviation calculated for the 19 average monthly sample sets.

As can be expected (Table 8), the fine particle volume percentages for deposition samples measured in the laboratory by Laser diffraction are much less than for the aerosol column measured by AERONET. In the former case (Table 8) the $\leq 10 \mu\text{m}$ of 7.51%, and $\leq 2.5 \mu\text{m}$ of 1.39%, as well as the $\leq 10 \mu\text{m} : \leq 2.5 \mu\text{m}$ average ratio of 1 : 0.19, are all substantially less than for the ambient AERONET measurements.

The approximate time series percentages and ratios for the AERONET samples are presented in Fig. 8. The missing monthly data for 25 of the 44 studied months in the four sampled years (2 months in 2016, 6 months in 2017, 8 months in 2018, 9 months in 2019) does not allow for a study of monthly or seasonal trends. However, there are increased fine fractions in the fall and early winter months of 2016, and 2018.

Gera. Please add to this discussion and results and perhaps something on subsequent and future research

Data Availability

The gravimetric, mineralogical and chemical data from this study are available upon request from Georgiy Stenchikov (Georgiy.Stenchikov@kaust.edu.sa).

Author Contributions

Johann Engelbrecht was responsible for the data analysis and compilation of the manuscript; Georgiy Stenchikov formulated the problem, designed the research project, and supported experimental activities; Iliia Shevchenko collected and conducted the sample preparation, freeze-drying of the samples, and performed the XRD analysis, and was also responsible for the AERONET optical site. Engelbrecht, Shevchenko, and Stenchikov compiled different parts of the manuscript.

Acknowledgements

This research, including the mineralogical analysis is supported by internal funding from the King Abdullah University of Science and Technology (KAUST). We acknowledge the contributions from the collaborating Core Labs at KAUST and the Desert Research Institute. This research is supported by the Supercomputing Laboratory at KAUST.

References

- Anisimov, A., Tao, W., Stenchikov, G., Kalenderski, S., Prakash, P. J., Yang, Z., and Shi, M.: Quantifying local-scale dust emission from the Arabian Red Sea coastal plain, *Atmospheric Chemistry and Physics*, 17, 993-1015, doi:10.5194/acp-17-993-2017, 2017.
- Bergametti, G., and Forêt, G.: Dust Deposition, in: *Mineral Dust. A Key Player in the Earth System*, edited by: Knippertz, P., and Stuut, J.-B. W., Springer, Dordrecht, 179-200, 2014.
- Biagio, C. D., Formenti, P., Balkanski, Y., Caponi, L., Cazaunau, M., Pangui, E., Journet, E., Nowak, S., Andreae, M. O., Kandler, K., Saeed, T., Piketh, S., Seibert, D., Williams, E., and Doussin, J.-F.: Complex refractive indices and single scattering albedo of global dust aerosols in the shortwave spectrum and relationship to iron content and size, *Atmospheric Chemistry and Physics Discussions*, <https://doi.org/10.5194/acp-2019-145>, 2019.
- Buseck, P. R., Jacob, D. J., Pósfai, M., Li, J., and Anderson, J. R.: Minerals in the air: An environmental perspective, *International Geology Review*, 42, 7, 577-593, doi: 10.1080/00206810009465101, 2000.
- Chung, F. H.: Quantitative interpretation of X-ray diffraction patterns of mixtures. I. Matrix-flushing method for quantitative multicomponent analysis, *Journal of Applied Crystallography*, 7, 519-525, doi:10.1107/S0021889874010375 1974.
- Comero, S., Capitani, L., and Gawlik, B. M.: Positive Matrix Factorisation (PMF), An introduction to the chemometric evaluation of environmental monitoring data using PMF, European Commission Joint Research Centre, Luxembourg: Office for Official Publications of the European Communities, 58, 2009.
- Edgell, H. S.: *Arabian Deserts. Nature, Origin and Evolution*, Springer, Dordrecht, Netherlands, 592 pp., 2006.
- Engelbrecht, J. P., McDonald, E. V., Gillies, J. A., Jayanty, R. K. M., Casuccio, G., and Gertler, A. W.: Characterizing mineral dusts and other aerosols from the Middle East – Part 1: Ambient sampling, *Inhalation Toxicology*, 21, 4, 297-326, doi: 10.1080/08958370802464273, 2009.
- Engelbrecht, J. P., and Jayanty, R. K. M.: Assessing sources of airborne mineral dust and other aerosols, in Iraq, *Aeolian Research*, 9, 153-160, 2013.
- Engelbrecht, J. P., Moosmüller, H., Pincock, S., Jayanty, R. K. M., Lersch, T., and Casuccio, G.: Technical Note: Mineralogical, chemical, morphological, and optical interrelationships of mineral dust re-suspensions, *Atmospheric Chemistry and Physics*, 16, 10809-10830, doi:10.5194/acp-16-10809-2016, 2016.
- Engelbrecht, J. P., Stenchikov, G., Prakash, P. J., Lersch, T., Anisimov, A., and Shevchenko, I.: Physical and chemical properties of deposited airborne particulates over the Arabian Red Sea coastal plain, *Atmospheric Chemistry and Physics*, 17, 11467-11490, <https://doi.org/10.5194/acp-17-11467-2017>, 2017.
- Ginoux, P., Prospero, J. M., Gill, T. E., Hsu, N. C., and Zhao, M.: Global-scale attribution of anthropogenic and natural dust sources and their emission rates based on MODIS Deep Blue aerosol products, *Reviews of Geophysics*, 50, 3, doi:10.1029/2012RG000388, 2012.
- Goossens, D., and Van Kerschaever, E.: Aeolian dust deposition on photovoltaic solar cells: The effects of wind velocity and airborne dust concentration on cell performance, *Solar Energy*, 66, 4, 277-289, 1999.
- Goudie, A. S., and Middleton, N.J.: *Desert Dust in the Global System*, Springer, 287 pp., 2006.

Hall, D. J., Upton, S. L., and Marsland, G. W.: Improvements in dust gauge design, in: *Measurements of Airborne Pollutants*, edited by: Couling, S., Butterworth, Heinemann, 1993.

Hamou, S., Zine, S., and Abdellah, R.: Efficiency of PV module under real working conditions, *Energy Procedia*, 50, 553-558, 2014.

Highwood, E. J., and Ryder, C. L.: Radiative effects of dust, in: *Mineral Dust, A Key Player in the Earth System*, edited by: Knippertz, P., and Stuut, J.-B. W., Springer, Dordrecht, 267-286, 2014.

Ilse, K., Werner, M., Naumann, V., Figgis, B. W., Hagendorf, C., and Bagdahn, J.: Microstructural analysis of the cementation process during soiling on glass surfaces in arid and semi-arid climates, *Physica Status Solidi RRL*, 1-5, doi: 10.1002/pssr.201600152, 2016.

Kalenderski, S., Stenchikov, G., and Zhao, C.: Modeling a typical winter-time dust event over the Arabian Peninsula and the Red Sea, *Atmospheric Chemistry and Physics*, 13, 1999-2014, doi:10.5194/acp-13-1999-2013, 2013.

Kalenderski, S., and Stenchikov, G.: High-resolution regional modeling of summertime transport and impact of African dust over the Red Sea and Arabian Peninsula, *Journal of Geophysical Research: Atmospheres*, 121, 6435-6458, doi:10.1002/2015JD024480, 2016.

Kandler, K., and Scheuevens, D.: Asian and Saharan dust from a chemical/mineralogical point of view: differences and similarities from bulk and single particle measurements, *E3S Web of Conferences, Central Asian Dust Conference (CADUC 2019)*, 99, 2019.

Mejia, F., Kleissl, J., and Bosch, J. L.: The effect of dust on solar photovoltaic systems, *Energy Procedia*, 49, 2370-2376, doi: 10.1016/j.egypro.2014.03.251, 2014.

Miller, R. L., Knippertz, P., Garcia-Pando, C. P., Perlwitz, J. P., and Tegen, I.: Impact of dust radiative forcing upon climate, in: *Mineral Dust, A Key Player in the Earth System*, edited by: Knippertz, P., and Stuut, J.-B. W., Springer, Dordrecht, 327-357, 2014.

Morman, S. A., and Plumlee, G. S.: Dust and human health, in: *Mineral Dust, A Key Player in the Earth System*, edited by: Knippertz, P., and Stuut, J.-B. W., Springer, Dordrecht, 385-409, 2014.

Muhs, D. R., Prospero, J. M., Baddock, M. C., and Gill, T. E.: Identifying sources of aeolian mineral dust: Present and past, in: *Mineral Dust, A Key Player in the Earth System*, edited by: Knippertz, P., and Stuut, J.-B. W., Springer Science+Business Media Dordrecht, 51-74, 2014.

Müller, D., Lee, K.-H., Gasteiger, J., Tesche, M., Weinzierl, B., Kandler, K., Müller, T., Toledano, C., Otto, S., Althausen, D., and Ansmann, A.: Comparison of optical and microphysical properties of pure Saharan mineral dust observed with AERONET Sun photometer, Raman lidar, and in situ instruments during SAMUM 2006, *Journal of Geophysical Research*, 117, D07211, doi:10.1029/2011JD016825, 2012.

Nenes, A., Murray, B., and Bougiatioti, A.: Mineral dust and its microphysical interactions with clouds, in: *Mineral Dust, A Key Player in the Earth System*, edited by: Knippertz, P., and Stuut, J.-B. W., Springer, Dordrecht, 287-325, 2014.

Nickovic, S., Vukovic, A., Vujadinovic, M., Djurdjevic, V., and Pejanovic, G.: Technical Note: High-resolution mineralogical database of dust-productive soils for atmospheric dust modeling, *Atmospheric Chemistry and Physics*, 12, 845-855, doi:10.5194/acp-12-845-2012, 2012.

Norris, G., Duvall, R., Brown, S., and Bai, S.: EPA Positive Matrix Factorization (PMF) 5.0 Fundamentals and User Guide, U.S. Environmental Protection Agency, 1-124, 2014.

- Paatero, P., and Tapper, U.: Positive matrix factorization: A non-negative factor model with optimal utilization of error estimates of data values, *Environmetrics*, 5, 111-126, 1994.
- Perlwitz, J. P., Pérez García-Pando, C., and Miller, R. L.: Predicting the mineral composition of dust aerosols – Part 1: Representing key processes, *Atmospheric Chemistry and Physics*, 15, 20, 11593–11627, doi: 10.5194/acp-15-11593-2015, 2015a.
- Perlwitz, J. P., Pérez García-Pando, C., and Miller, R. L.: Predicting the mineral composition of dust aerosols – Part 2: Model evaluation and identification of key processes with observations, *Atmospheric Chemistry and Physics*, 15, 20, 11629-11652, doi: 10.5194/acp-15-11629-2015, 2015b.
- Prakash, P. J., Stenchikov, G., Tao, W., Yapici, T., Warsama, B., and Engelbrecht, J. P.: Arabian Red Sea coastal soils as potential mineral dust sources, *Atmospheric Chemistry and Physics*, 16, 18, 11991-12004, doi:10.5194/acp-16-11991-2016, 2016.
- Prospero, J. M., Ginoux, P., Torres, O., Nicholson, S. E., and Gill, T. E.: Environmental characterization of global sources of atmospheric soil dust identified with the Nimbus 7 Total Ozone Mapping Spectrometer (TOMS) absorbing aerosol product, *Reviews of Geophysics*, 40, 1, doi:10.1029/2000RG000095, 2002.
- Rao, A., Pillai, R., Mani, M., and Ramamurthy, P.: Influence of dust deposition on photovoltaic panel performance, *Energy Procedia*, 54, 690-700, doi: 10.1016/j.egypro.2014.07.310, 2014.
- Scanza, R. A., Mahowald, N., Ghan, S., Zender, C. S., Kok, J. F., Liu, X., Zhang, Y., and Albani, S.: Modeling dust as component minerals in the Community Atmosphere Model: development of framework and impact on radiative forcing, *Atmospheric Chemistry and Physics*, 15, 537-561, doi:10.5194/acp-15-537-2015, 2015.
- Scheuvens, D., and Kandler, K.: On composition, morphology, and size distribution of airborne mineral dust, in: *Mineral Dust, a Key Player in the Earth System*, edited by: Knippertz, P., and Stuut, J.-B. W., Springer Science+Business Media Dordrecht, 15-49, 2014.
- Schulz, M., Prospero, J. M., Baker, A. R., Dentener, F., Ickes, L., Liss, P. S., Mahowald, N. M., Nickovic, S., García-Pando, C. P., Rodríguez, S., Sarin, M., Tegen, I., and Duce, R. A.: Atmospheric transport and deposition of mineral dust to the ocean: implications for research needs, *Environmental Science & Technology*, 46, 19, 10390-10404, doi: 10.1021/es300073u, 2012.
- Sulaiman, S. A., Singh, A. K., Mokhtar, M. M. M., and Bou-Rabee, M. A.: Influence of dirt accumulation on performance of PV panels, *Energy Procedia*, 50, 50-56, doi: 10.1016/j.egypro.2014.06.006, 2014.
- Vallack, H. W., and Chadwick, M. J.: A field comparison of dust deposit gauge performance at two sites in Yorkshire, *Atmospheric Environment Part A*, 26, 8, 1445-1451, [https://doi.org/10.1016/0960-1686\(92\)90129-9](https://doi.org/10.1016/0960-1686(92)90129-9), 1992.
- Vallack, H. W., and Chadwick, M. J.: Monitoring airborne dust in a high density coal-fired power station region in North Yorkshire, *Environmental Pollution*, 80, 2, 177-183, [https://doi.org/10.1016/0269-7491\(93\)90145-E](https://doi.org/10.1016/0269-7491(93)90145-E), 1993.
- Vallack, H. W.: A field evaluation of Frisbee-type dust deposit gauges, *Atmospheric Environment*, 29, 12, 1465-1469, [https://doi.org/10.1016/1352-2310\(95\)00079-E](https://doi.org/10.1016/1352-2310(95)00079-E), 1995a.
- Vallack, H. W.: Protocol for using the dry Frisbee (with foam insert) dust deposit gauge, SEI (Stockholm Environment Institute), 1995b.
- Vallack, H. W., and Shillito, D. E.: Suggested guidelines for deposited ambient dust, *Atmospheric Environment*, 32, 16, 2737-2744, [http://doi.org/10.1016/S1352-2310\(98\)00037-5](http://doi.org/10.1016/S1352-2310(98)00037-5), 1998.

Washington, R., and Todd, M. C.: Atmospheric controls on mineral dust emission from the Bodélé depression, Chad: The role of the low level jet, *Geophysical Research Letters*, 32, L17701,, doi:10.1029/2005GL023597, 2005.